Gase, A.C., et al., 2022, Hikurangi megathrust slip behavior influenced by lateral variability in sediment subduction: Geology, v. 50, https://doi.org/10.1130/G50261.1

SUPPLEMENTAL MATERIAL

Hikurangi megathrust slip behavior influenced by lateral variability in sediment subduction

Andrew C. Gase[1*], Nathan L. Bangs[1], Harm J. A. Van Avendonk[1], Dan Bassett[2], Stuart A. Henrys[2]

[1] *Institute for Geophysics, Jackson School of Geosciences, University of Texas at Austin, Austin Texas, 78758, USA*

[2] *GNS Science, PO BOX 30368, Lower Hutt 5040, New Zealand*

Contact: Andrew Gase, Email: agase@utexas.edu

SHIRE SEISMIC DATA ACQUISITION AND PROCESSING

In 2017, the R/V *Langseth* acquired 4,046 line-km of multichannel seismic reflection data along the Hikurangi margin (MGL1708) during the Seismogenesis at Hikurangi Integrated Research Experiment (SHIRE). For the SHIRE seismic data presented here, shots were generated at 50 m intervals with a 6,600 in^3 tuned air-gun array. Resulting seismic energy was recorded with an ultra-long 12.5 km, 1,008 channel solid-state hydrophone streamer with 12.5 m hydrophone spacing. The seismic source and hydrophone streamer were towed below the sea-surface at 9 m and 12.5 m, respectively.

The goal of our seismic processing strategy was to image the Hikurangi forearc and deeper plate boundary zone. We use the same approach as Gase et al., (2021): the seismic data were (1) sampled at 4 ms, (2) bandpass frequency filtered to reduce ocean swell noise (1-2-60-100 Hz), and (3) trace balanced. Next, we applied surface-related multiple elimination and radon filtering to attenuate strong seafloor multiple arrivals. This multiple elimination strategy was most successful in areas with smooth topography (e.g., slope basins) and occasionally failed to remove multiple energy near irregular topographic features (e.g., thrust ridges). Our target region (>3 km bsf) is well beyond depths that can be imaged with streamer tomography on a 12.5 km streamer (generally <3 km bsf). We relied on conventional normal move-out seismic velocity analysis to build velocity models for seismic migration. Velocities were further constrained with iterations of pre-stack depth migration. To produce final seismic images, we performed Kirchhoff pre-stack time and depth migrations (Figs. 2 and 3). After migration, we applied inside and outside mutes to common image gathers and stacked the migrated traces to produce seismic sections.

Hikurangi Margin Seismic Stratigraphy

Seismic stratigraphy on the Hikurangi Plateau is uncertain due to a lack of deep-water drilling data that provide lithological and biostratigraphic age controls. IODP Expedition 372B/375 provides age and lithological constraints through the incoming Hikurangi Plateau sediments offshore the northern Hikurangi margin (Barnes et al., 2019). Several seismic stratigraphic frameworks exist for the offshore stratigraphy of the Hikurangi margin (Davy et al., 2008; Barnes et al., 2010; Bland et al., 2015). These frameworks identify common features including unconformities and laterally continuous, strong reflectors but disagree with regards to the age associated with several horizons. Rather than pick individual horizons within a single framework, we identify three major horizons that are commonly identified within all of the above frameworks to guide our interpretation of the incoming plate stratigraphy. In upward stratigraphic order these include:

(Horizon 1) The top of Cretaceous Hikurangi Plateau volcanics (~120-80 Ma) is commonly marked by a strong, irregular reflection, occasional minor volcanic cones, and major seamounts. This horizon is referred to as H in Bland et al. (2015), Reflector 8 in Barnes et al. (2010), and the top of VB and HKB in Davy et al. (2008).

(Horizon 2) A strong reflector immediately below the proto-décollement that is thought to separate Cretaceous siliciclastic siltstones and sandstones from Paleocene-Eocene pelagic carbonates. This horizon coincides with the top of Unit MES in Davy et al. (2008), the base of the Eocene within Unit 3B in Bland et al. (2015), and the base of Sequence-Y (inferred late Mesozoic) in Barnes et al. (2010). We interpret this horizon as the top of sediments beneath the proto-décollement.

(Horizon 3) We also interpret a margin-wide unconformity that separates middle to lower Pleistocene marls and mudstones from middle to lower Pleistocene and younger hemipelagic turbidites (Barnes et al., 2019). Barnes et al. (2010) refer to this horizon as Reflector 5b, whereas Bland et al. (2015) identify this horizon to separate their Units 4A and 4B.

We use the above horizons to identify four seismic-stratigraphic units that include the Hikurangi Plateau (HKB), subducting sediments and sediments beneath the proto-décollement (MES), calcareous sediments (CL), and siliciclastic trench-fill sediments (TF).

We use legacy seismic data within the study area to estimate the thickness of unit MES. Key acquisition parameters for data quality are presented in Table S1. Legacy data were only used where the key horizons could be confidently interpreted. We picked the three key horizons and the seafloor reflection on the SHIRE seismic lines as well as legacy single and multi-channel seismic lines (Figs. S3, S4, S6). Seismic velocities strongly depend on lithology, stress, and cementation. With seismic datasets of varying quality and velocity control it is unfeasible to account for seismic velocity heterogeneity at the stratigraphic scale across the margin. To estimate apparent sediment thickness, we use a one-dimensional P-wave velocity function acquired within the Pegasus Basin

(Mochizuki et al., 2019) and convert traveltime picks to depth. Finally, we create an apparent sediment thickness map of Unit MES by subtracting the depths of Horizons 1 and 2 and applying a nearest neighbor interpolation with 40 km maximum range (Fig. 4).

REFERENCES FOR SUPPLEMENTAL MATERIAL:

Anardarko New Zealand Ltd, 2014, APB-13–2D Pegasus Basin 2D quality assurance report PEP 54861 marine 2D seismic survey PEP 54858. NZP&M, Ministry of Business, Innovation & Employment (MBIE), New Zealand unpublished petroleum report PR5172.

Barnes, P.M. et al., 2019, Site U1520, *in* Hikurangi Subduction Margin Coring, Logging, and Observatories, College Station, TX, Proceedings of the International Ocean Discovery Program, v. 372B/375, doi:10.14379/iodp.proc.372B375.105.2019.

Barnes, P.M., Lamarche, G., Bialas, J., Henrys, S., Pecher, I., Netzeband, G.L., Greinert, J., Mountjoy, J.J., Pedley, K., and Crutchley, G., 2010, Tectonic and geological framework for gas hydrates and cold seeps on the Hikurangi subduction margin, New Zealand: Marine Geology, v. 272, p. 26–48, doi:10.1016/j.margeo.2009.03.012.

Bialas, J., 2011, FS Sonne Fahrtbericht/Cruise Report SO214 NEMESYS: 09.03-05.04 (9 March - 5 April) 2011, Wellington - Wellington; 06.-22.04 (6-22 April) 2011 Wellington - Auckland: IFM-GEOMAR Report 47, p. 174.

Bland, K.J., Uruski, C.I., and Isaac, M.J., 2015, Pegasus Basin, eastern New Zealand: A stratigraphic record of subsidence and subduction, ancient and modern: New Zealand Journal of Geology and Geophysics, v. 58, p. 319–343, doi:10.1080/00288306.2015.1076862.

Collot, J. -Y, Delteil, J., Herzer, R.H., Wood, R., and Lewis, K., 1995, Sonic imaging reveals new plate boundary structures offshore New Zealand: Eos, Transactions American Geophysical Union, v. 76, p. 1–5, doi:10.1029/EO076i001p00001-01.

Davey, F.J., Hampton, M., Childs, J., Fisher, M.A., Lewis, K., and Pettinga, J.R., 1986, Structure of a growing accretionary prism, Hikurangi margin, New Zealand: Geology, v. 14, p. 663–666, doi:10.1130/0091-7613(1986)14<663:SOAGAP>2.0.CO;2.

Davy, B., Hoernle, K., and Werner, R., 2008, Hikurangi Plateau: Crustal structure, rifted formation, and Gondwana subduction history: Geochemistry, Geophysics, Geosystems, v. 9, doi:10.1029/2007GC001855.

Gase, A.C. et al., 2021, Crustal Structure of the Northern Hikurangi Margin, New Zealand: Variable Accretion and Overthrusting Plate Strength Influenced by Rough Subduction: Journal of Geophysical Research: Solid Earth, v. 126, p. 1–26, doi:10.1029/2020JB021176.

Mobil 1972 Seismic profiles along the East Coast North Island, and the Kermadec-Tonga Island Arc to Fiji. New Zealand Geological Survey. Unpublished open file petroleum report 587.

Mochizuki, K. et al., 2019, Recycling of depleted continental mantle by subduction and plumes at the Hikurangi Plateau large igneous province, southwestern Pacific Ocean: Geology, v. 47, p. 795–798, doi:10.1130/G46250.1.

RPS Energy, 2010, Pegasus Basin, Bounty Trough and SAHKE seismic - Report on contractor's performance during 2D seismic survey 13th November 2009 to 30th March 2010. Ministry of Economic Development New Zealand unpublished petroleum report PR 4158.:

Wood, R.A., and Anderson, H.J., 1989, Basement structure at the Chatham Islands: Journal of the Royal Society of New Zealand, v. 19, p. 269–282, doi:10.1080/03036758.1989.10427182.

SUPPLEMENTAL FIGURES:

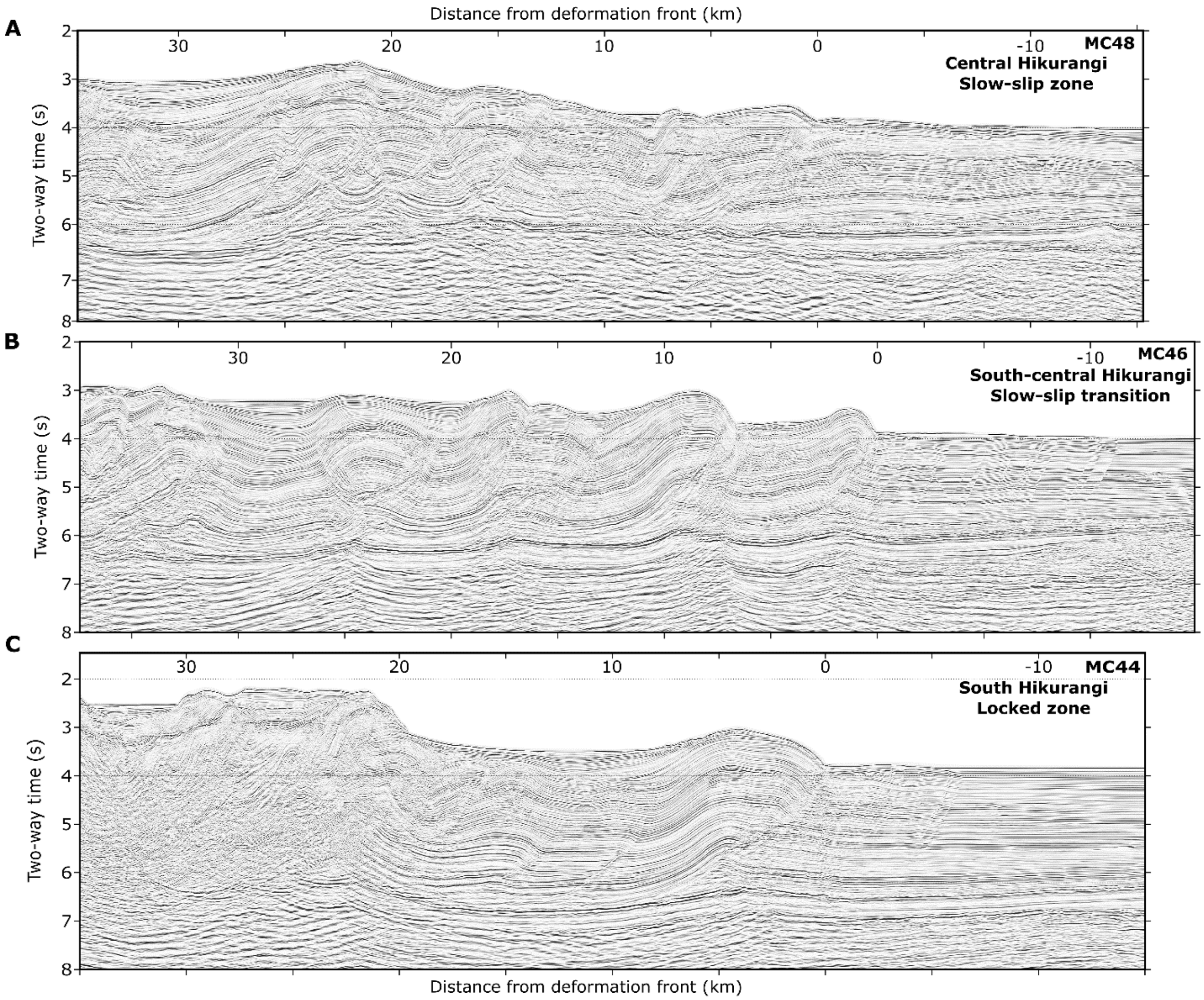

Figure S1. Uninterpreted pre-stack time-migrated reflection images of the frontal prism zone of MC48, MC46, and MC44.

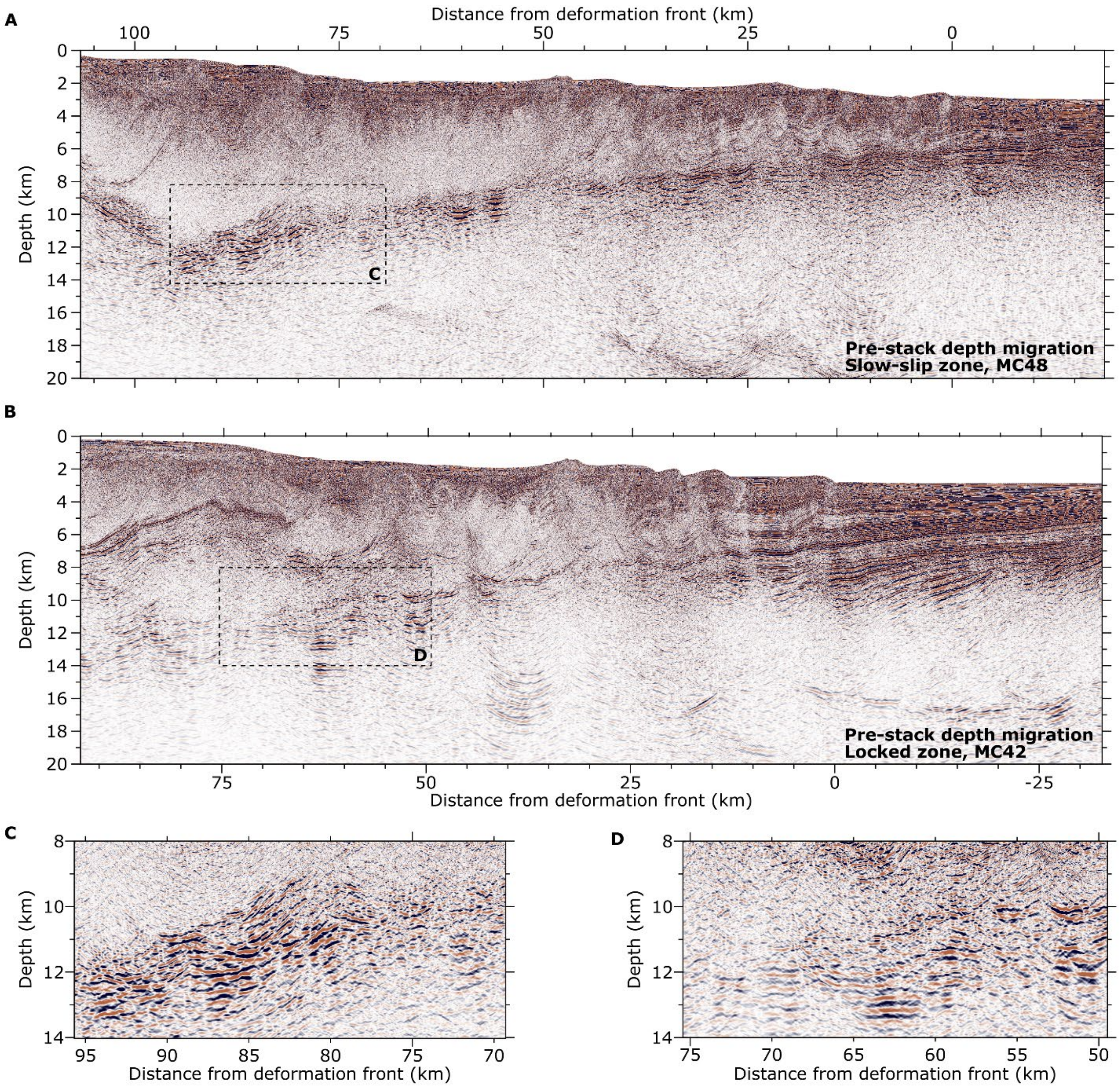

Figure S2. Uninterpreted pre-stack depth-migrated reflection images of the MC48, and MC42.

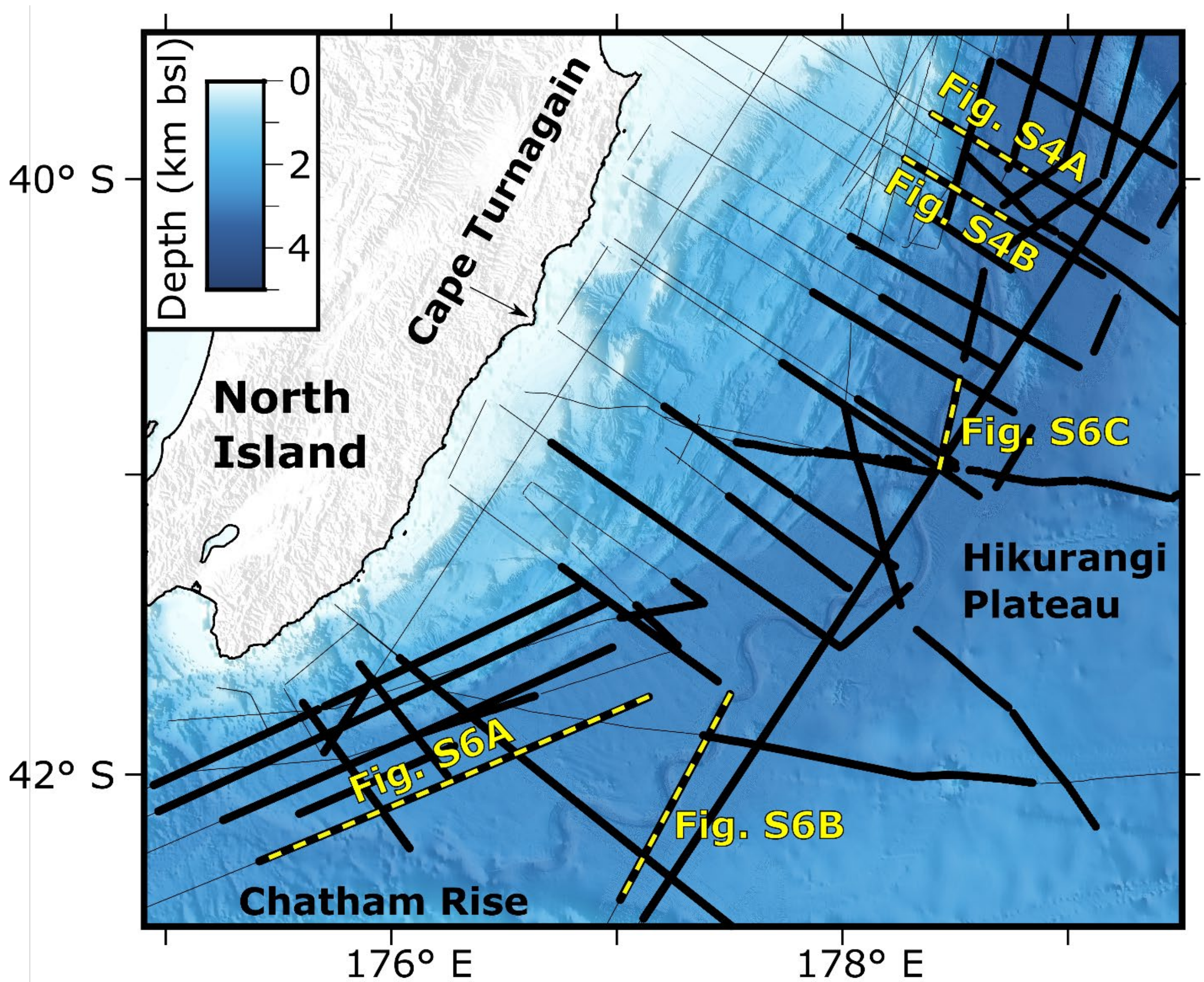

Figure S3. Map of SHIRE and legacy seismic lines. Bold lines indicate locations of picks used to estimate the thickness of MES shown in Fig. 4.

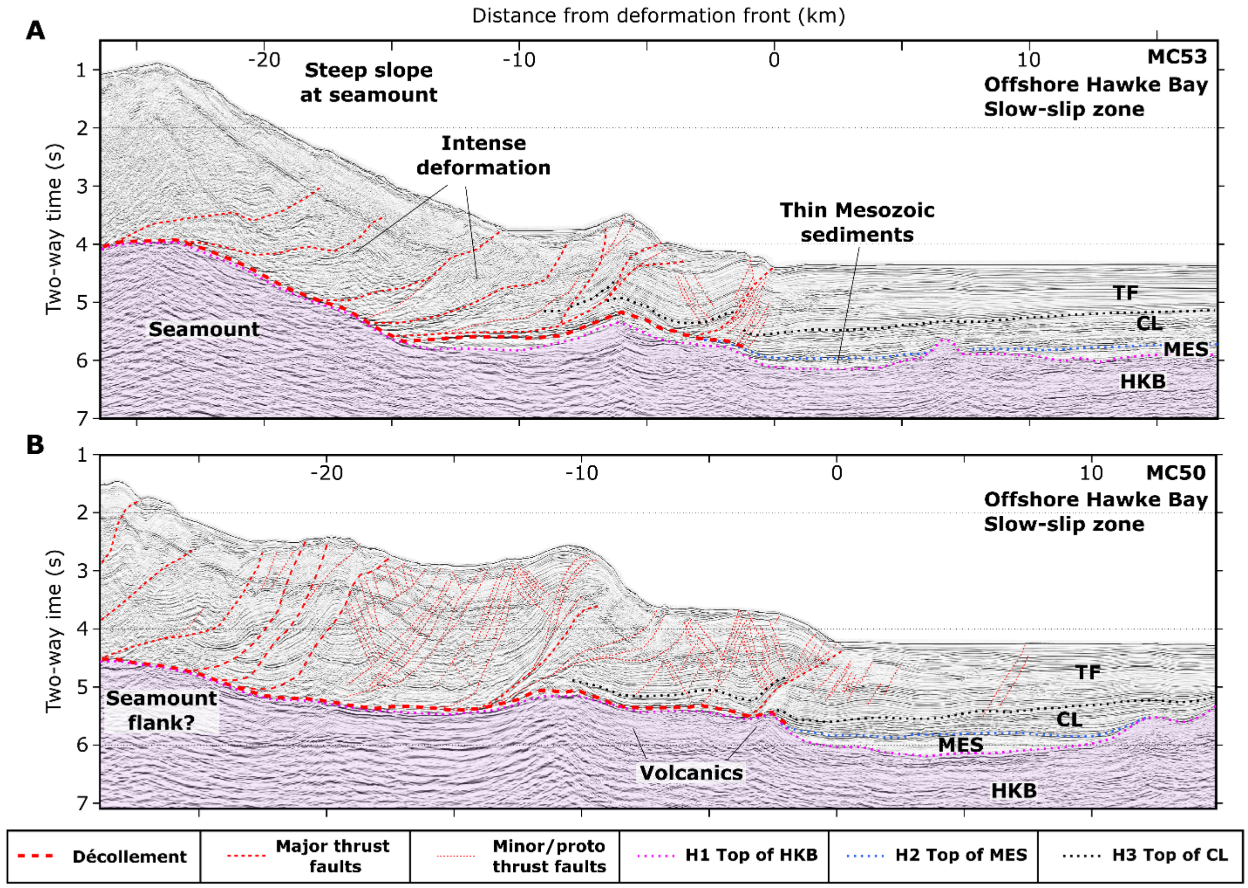

Figure S4. Pre-stack time-migrated reflection images of the frontal prism zone of MC53 and MC50.

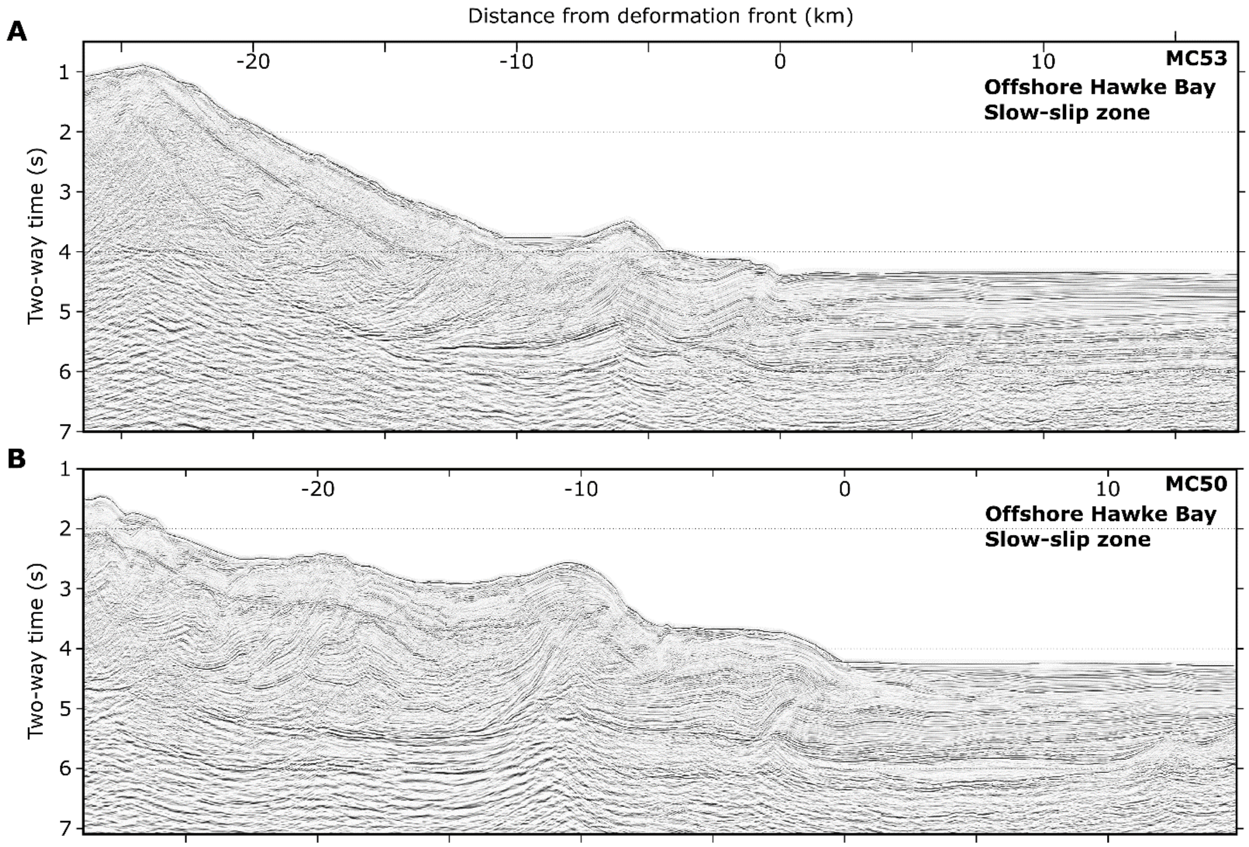

Figure S5. Uninterpreted pre-stack time-migrated reflection images of the frontal prism zone of MC53 and MC50.

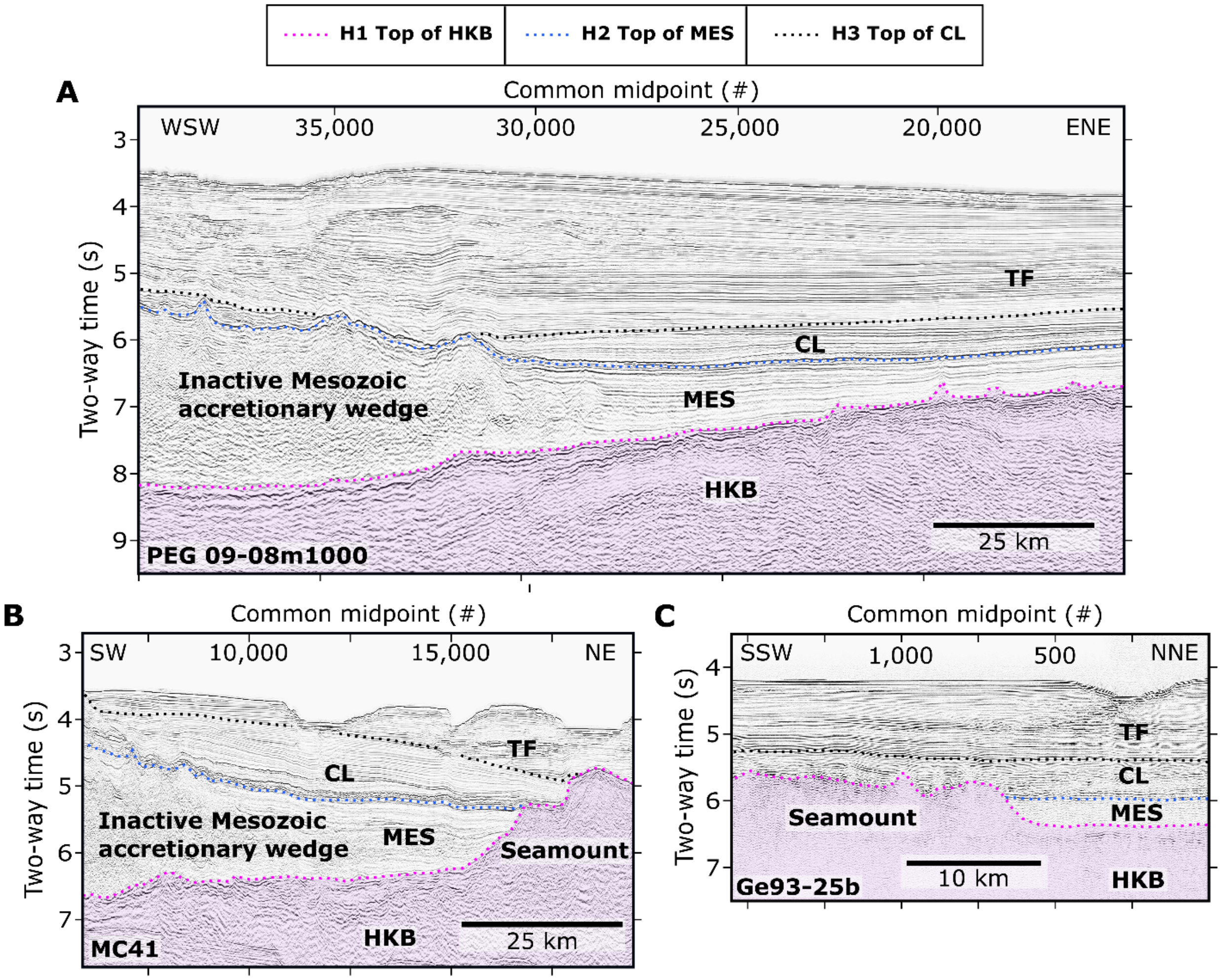

Figure S6. Reflection images of PEG 09-08m1000, MC41, and Ge93-25b on the incoming plate.

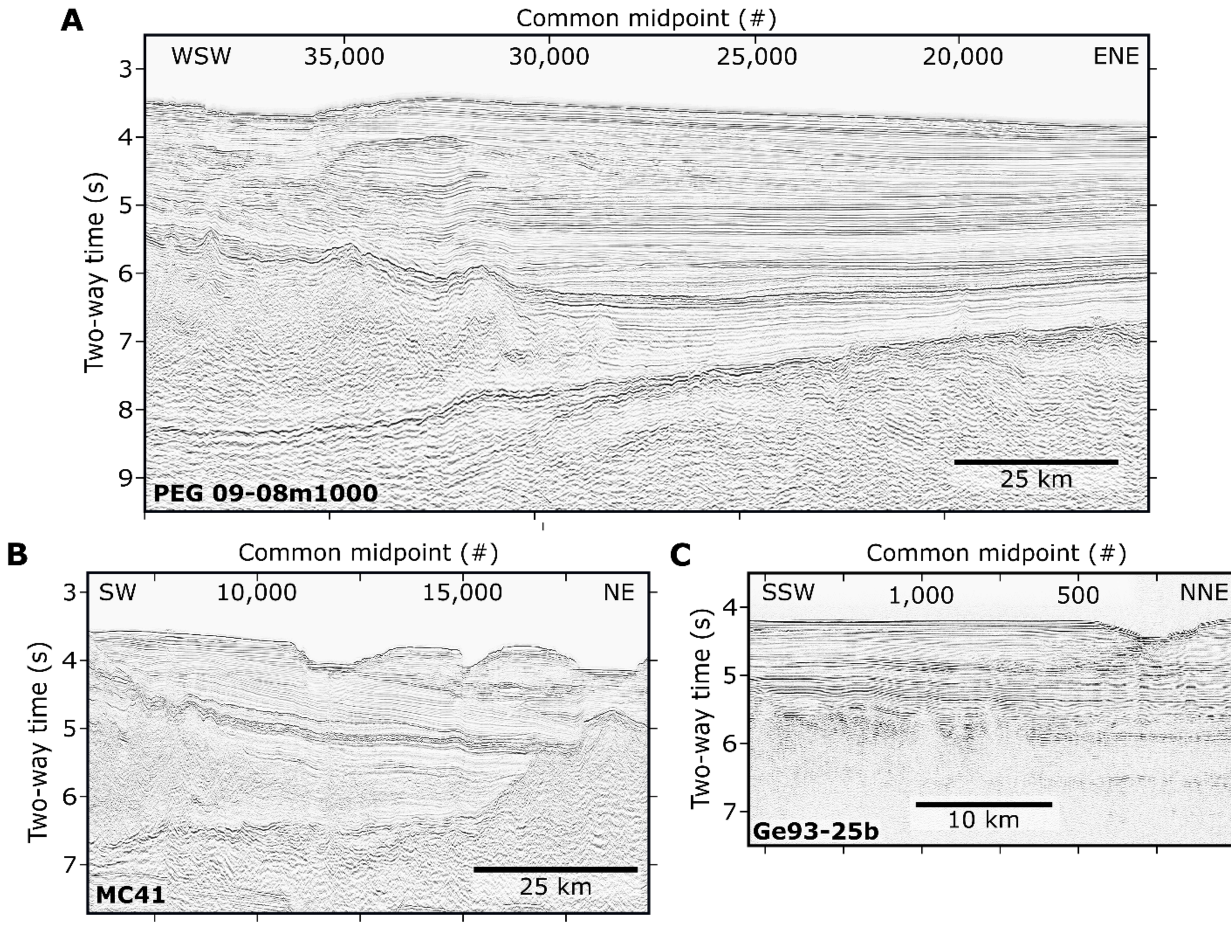

Figure S7. Uninterpreted reflection images of PEG 09-08m1000, MC41, and Ge93-25b on the incoming plate.

SUPPLEMENTAL TABLE

Table S1. Key acquisition parameters for seismic data

Survey Name	Organization	Reference	Streamer length (km)	Channels	Source
APB 13	Anadarko	Anardarko New Zealand Ltd, 2014	8.1	648	3,610 cu inch tuned airgun array
BT8203	DSIR Geophysics Division	Wood and Anderson, 1989	0.1	1	120 cu in Bolt airgun
GEODY NZ-SUD (Ge93)	Institut Francais de Recherche pour l'Exloitation de la Mer (IFREMER)	Collot et al., 1995	N. A.	6	2 x 75 cu inch GI guns
Mobil-72	Mobil Oil	Mobil, 1972	1.425	24	4 x 1,560 cu inch airguns
NIGHT	GNS-Science	Henrys et al., 2006	6.0	480	8,200 cu inch airgun
PEG09	New Zealand Government	RPS Energy, 2010	10.1	800	5,400 cu inch tuned airgun array
SHIRE	U.S. National Science Foundation	Gase et al., 2021	12.5	1,008	6,600 cu inch tuned airgun array
SOL, Sonne 191	GEOMAR/NIWA	Bialas, 2011	0.6	32-48	4 x 520 cu inch airguns
SP Lee	DSIR Geophysics Division	Davey et al., 1986	2.4	24	5 x 260 cu inch airguns